Indian Journal of Engineering & Materials Sciences
Vol. 31, April 2024, pp. 245-257
DOI: 10.56042/ijems.v31i2.1034

Aerodynamic and aeroelastic response of wind barrier over trapezoidal box girder bridge under turbulence wind

*Puja Haldar & Somnath Karmakar

Department of Civil Engineering, National Institute of Technology, Durgapur 713 209, India

Received: 30 April 2023; Accepted: 22 January 2024

Dynamic loadings, such as earthquakes, blasts, and wind, may be unanticipated for a bridge during its design phase, which is the essential infrastructure in the transport system. Therefore, wind barriers associated with the bridge deck could adversely impact the dynamic stability and require to be designed under extreme wind impact. Fortunately, the research said innovative materials improve performance under high dynamic loads. In the present study, incompressible computational fluid dynamic has been adopted to explore the aerodynamic and aeroelastic responses of a Trapezoidal box girder bridge deck section for several materials based solid wind barriers: Normal concrete, crumb rubber concrete, alcofine-based crumb rubber concrete, silica fume-based crumb rubber concrete and glass fibre-reinforced polymer concrete. The improved material features help to use innovative, sustainable alcofine-based crumb rubber concrete as a catalyst in solid wind barriers. The bridge deck does not exhibit any significant changes in aerodynamic characteristics. Under turbulent wind, the wind barrier on the deck section is more resilient to the vortex. The shear layers separate from the wind barrier's top, influencing the torsional moment and the bridge deck dynamics. Finally, alcofine-based crumb rubber concrete improves the wind resistance capacity of the wind barrier.

Keywords: Trapezoidal box girder bridge, Solid wind barriers, Incompressible computational fluid dynamics, Input energy, Torsional displacement, Heaving displacement

1 Introduction

The developments of natural hazards like cyclones, floods, earthquakes, landslides, and pestilences are becoming frequent and common, appearing at any time in any part of the globe[1, 2]. Among them, the mitigation of the cyclonic epidemic now become an international concern due to its terrible disasters. In contrast to an earthquake, the average life of a cyclone is approximately five days from the time of creation to landfall. Conversely, an earthquake happens rapidly and unpredictably[3, 4]. The Indian state of West Bengal (WB) is situated in the lap of the Bay of Bengal (BOB): part of the Indian Ocean, perhaps one of the world's six dangerous cyclonic provinces. However, the maximum basic wind speed zone endorsed by the Indian code for the structural design is 55 m/s. Again, 61.6 m/s is the highest supercyclonic wind speed reported by the Indian Meteorological Department (IMD) till date[5]. Another attention attracting severe concern is the safety of high-speed vehicles on highways and railways under robust crosswinds associated with bridges. Vehicles can collide with structural elements or each other and also overturn due to these adverse wind effects. Monitoring and warning systems for strong wind, shape optimisation of vehicles, and construction of wind barriers are the typical three mitigation approaches to reduce wind loads. The critical factors are maintenance cost, long-term reliability, and accuracy prediction for monitoring systems. The shape optimisation approach is associated with the new design of vehicles. The roadway wind barrier design is an excellent option among several mitigation approaches[6, 7]. However, flutter, vortex-induced Vibration (VIV), buffeting, and galloping are the four main wind induced vibration (WIV) categories that consider wind mechanisms. Catastrophic failure mainly happens for flutter, whereas buffeting, VIV, etc., accomplish fatigue failure 8. The chances of flutter are low; therefore, mitigating fatigue problems on wind barriers due to these types of winds is indispensable.

Conversely, much attention has been paid to the alternative reuse of waste materials from many sources[9-16]. One of those that is not naturally biodegradable is the waste tyre. Approximately 1.5 billion discarded tyres are disposed of annually[17]. An alarm for our civilisation is that the number will be

*Corresponding author (E-mail: ph.19ce1103@phd.nitdgp.ac.in)

extended to 5 billion by 203018.This waste can become a mosquito habitat due to its water proof nature and shape. Since 1990, waste tyres, with their crumb form, have been utilised as a modifier in their initial application[19]. This approach has been extended to concrete, popularly known as Crumb Rubber Concrete (CRC). However, alccofine and silica fume are sophisticated materials for enhancing CRC strength, considering the microscale voids within CRC 20. Numerous experiments show that adding innovative material to concrete improved strength[21, 22, 23, 24, 25,26]. Thus, the research has concentrated on searching for the efficiency of CRC with alccofine as an application to wind barriers.

Wind loads are more likely to happen over the infrastructure; therefore, it is crucial to consider this when designing the structures. The different forms of WIV and their coupling have been studied to understand the behaviour of bridges. It was observed that buffeting, galloping, and VIV are responsible for fatigue, which is required to nullify the desired performance of the bridge. Fortunately, prior research has shown innovative materials react more positively to dynamic loading. Therefore, the present study intends to enhance the elastic property of solid wind barriers (SWB) using various materials: Normal Concrete (NC), CRC, Alcofine-based Crumb Rubber Concrete (AbCRC), Silica fume-based Crumb Rubber Concrete (SLCRC) and Glass Fibre-Reinforced Polymer Concrete (GFRP)using Incompressible Computational Fluid Dynamics (ICFD).

The present study considers data from previous cyclones originating from the Indian Ocean. The implicit numerical analysis has been completed with a double-precision Reynolds-averaged Navier–Stokes (RANS) based ICFD solver using Ansys LS-DYNA. Finally, the SWB of the deck using AbCRC plays a good role under extreme winds.

The parallel and perpendicular forces to the flow are called Drag (FD) and lift (FL) when a body is subjected to wind. The respective moment (M) along the horizontal axis of the structure is called the Torsional Moment. These are the sway or horizontal force (FH) along with the horizontal axes and the vertical force (FV) along with the normal axes in a structural coordinate system.However, these may be expressed using air density (ρ), oncoming wind velocity (U), deck width (B), span-wise deck length (L), and the bridge deck depth (D). Figure 1 shows the forces and moment direction on a bridge cross-section.

Equations (1-4) signify the formulation of the Drag Coefficient (CD), Lift Coefficient (CL) and Moment Coefficient (CM)[27]. Therefore,

$$F_D = 0.5\rho U^2 C_D DL \quad \ldots (1)$$

$$\text{Clearly, } C_D = \frac{F_D}{0.5\rho U^2 DL} \quad \ldots (2)$$

$$\text{Similarly, } C_L = \frac{F_L}{0.5\rho U^2 BL} \quad \ldots (3)$$

$$C_M = \frac{M}{0.5\rho U^2 B^2 L} \quad \ldots (4)$$

2 Materials and Methods

2.1 Materials, wind speed and research process

Figure 2(a) shows the entire process of the present numerical analysis. The SWB of NC, AbCRC, CRC, SLCRC, and GFRP models have been implicitly analysed to check the Aerodynamic force. Table 1 describes the material details and air properties used in the ICFD[22].The two specific wind velocities (61.1 and 47 m/s) have been considered based on metrological observations and code references noticing the bridge location[5, 28]. However, the models have been named by an abbreviation like 10M_AbCRC, which means 10 mesh (hole per inch) size Crumb Rubber (CR) used in AbCRC. A continuous surface cap model has been applied to the concrete[29, 30].

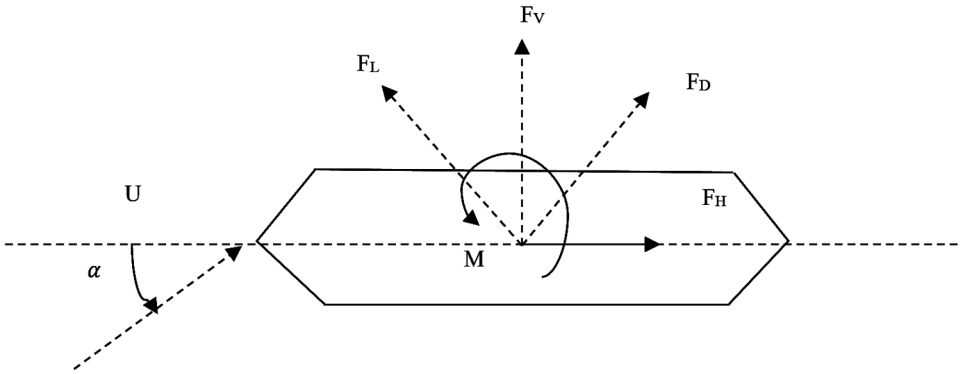

Fig. 1 — Force and moment direction on trapezoidal box girder bridge (TBGB).

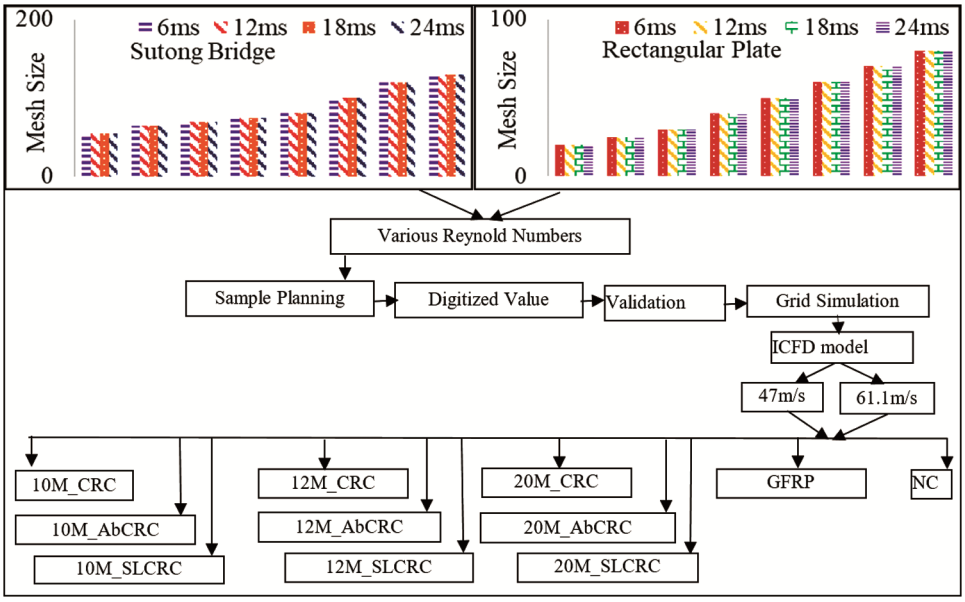

Fig. 2(a) — Steps of numerical analysis.

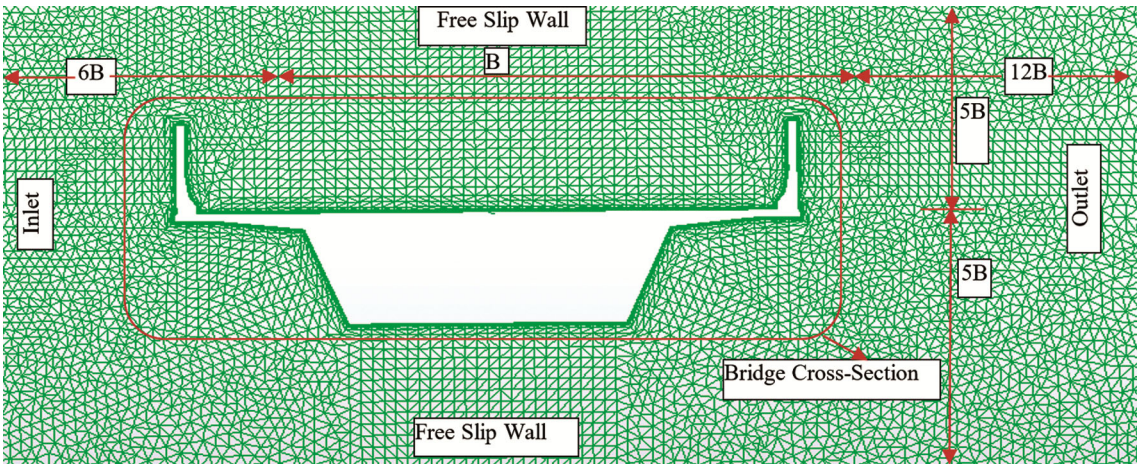

Fig. 2(b) — Boundary conditions and computational domain(23, 24).

Table 1 — Material properties used in the ICFD material model.

Material	Material Name	Ec (GPa)	Density (kg/m3)	Poisson's Ratio
Bridge	NC	27.95	2400	0.160
	CRC	27.15	1800	0.150
	AbCRC	29.82	1800	0.200
	SLCRC	23.86	1800	0.150
	GFRP	08.60	1250	0.183
Air	Dynamic Viscosity 1.849x10-05 (kg/m-s)	Initial Turbulence 5% Intensity	Flow Density 1.184	Fluid Type Fully Incompressible

2.2 Boundary condition and computational domain

Figure 2(b) shows the boundary condition of the computational domain with a typical bridge cross-section, having 'B' as the cross-sectional width. The 12B and 6B are the rare faces to the outlet and the leading edge to the inlet distance of the model[31], 32. Similarly, to limit less than a 3% blocking ratio, 10B has been retained between the top and bottom of the domain. These numbers have been chosen to guarantee the boundary's independent inlet condition, which allows the inlet's turbulent wake to proceed. Therefore, 5% turbulence intensity has been accepted for the inlet. The outlet boundary is also connected to the outlet pressure and zero relative pressure. Free-

slip boundaries surround the top and bottom walls. A no-slip wall boundary is around the surface of the section. Again, both ends of the model are accompanied by a symmetrical limit. The present work continued with triangular meshing.

2.3 Numerical establishment

In the context of computational speed and cost reduction, the best option is numerical simulation. In real-world problems, mathematical algorithms function well. However, verifying the results compared to the system behaviour is doubtful. How does it measure how closely the simulations match reality? In this regard, before determining the response of the bridge deck under different wind flows using the ICFD, it is vital to verify the accuracy of the techniques. The cross-section of the Sutong bridge and a rectangular plate have been taken to verify the model. The cross-sectional sections of the model have a total width of 0.585 m, and their length is 1 m. The full-size bridge section is used only at a geometric scale of 1:70, significantly decreasing the computational effects 33. The bridge and rectangular plate cross-section's pressure drag coefficient (CDP) and friction drag coefficient (CDF) for various reynolds numbers (Re) have been digitised in Figures 2(c–d), and the present numerical simulation results[33, 34]. Figures 2(e-f) describe the simulation results for the same structures on relevant meshes. There is a grantable agreement in the digitised version of the experimental with present numerical simulation results and ICFD results for identical cross-sections, which is optimistic.

Moreover, a 750 mm mesh size has been obtained by mesh sensitivity analysis as an optimised mesh for the present works. Considering static loading conditions, the bridge reactionis quantitatively evaluated and compared with the assessment of fundamental frequency and displacement, producing a good confirmation, as shown in Table 2[35]. Unsteady reynolds averaged navier-stokes (URANS) simulations have been performed using the k-ω SST model, and the adopted time-step is 0.01 s. The whole simulation has been conducted using the ICFD Ansys LS-Dyna subroutine.

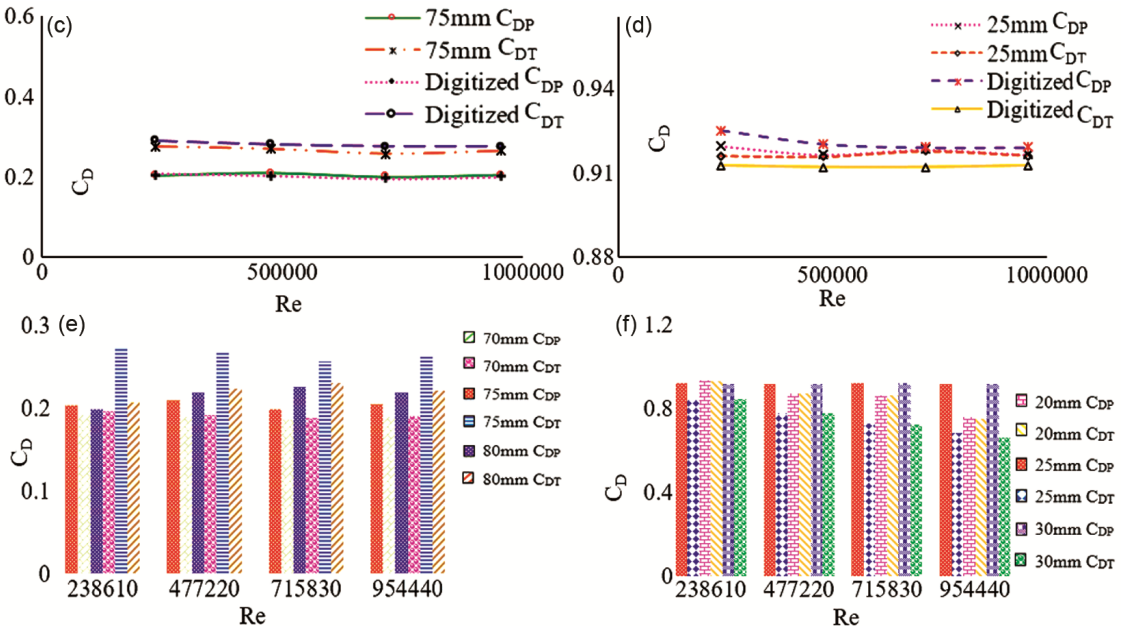

Fig. 2 — (c) CD of sutong bridge, (d) CD of rectangular plate, (e) Sutong bridge grid simulation, & (f) rectangular plate grid simulation.

Table 2 — Validation of bridge response 35.

Description	Computed Result	Theoretical Result
Fundamental frequency for Bridge self-weight	2.9952Hz	2.88Hz
Fundamental Frequency (at 100 kN mass)	23Hz	20.69Hz
Static Deflection,	0.553 mm	0.59mm
a) At mid		
b) At 1/4th L from the support (L= Bridge length)	0.366 mm	0.33mm
c) At 1/8th L from the support	0.12 mm	0.112mm

3 Results and Discussion

3.1 Effect of aerodynamic forces and moment

As discussed, the numerical simulation has been performed on a single-deck TBGB with various wind barrier materials (WBM) and two specific wind velocities. Figure 3(a-c) shows the drag force, lift force and moment coefficient for various ICFD models for multiple materials and wind Speeds. The CD value of the 20M_AbCRC, 20M_CRC and 20M_SLCRCSWB bridge deck is only 0.5%, 0.23% and 0.9% more than the NC for 47m/s wind speed and 0.5%, 2.1% and 1.2% more than the NC for 61.1 m/s wind speed. This minimal increment justifies that the aerodynamic FD does not effectively influence CD for the material variation on the SWB. The maximum CL value decreases by 20% and 5% for 12M_SLCRC and 20M_CRC compared to NC for 47m/s and 61.1m/s wind speed.Conversely, the CL value variation of 20M_AbCRC, 20M_CRC, and 20M_SLCRC SWB bridge deck is only 1.4%, 0.5% decrease and 2.5% increase than the NC for 47m/s wind speed and 14 % increase,5.5% decrease and 15.5% increase than the NC for 61.1 m/s wind speed.

The maximum CM value decreases by 14% and 6.1% for 12M_CRC and 20M_CRC compared to NC for 47m/s and 61.1m/s wind speed. Again, the CM value of 20M_AbCRC, 20M_CRC and 20M_SLCRC SWB bridge deck is only 0.4%, 0.4% and 2.4% more than the NC for 47m/s wind speed and 3.6%, 6.1% and 4.9% more than the NC for 61.1 m/s wind speed. The drag force is the summation of pressure and frictional drag force. The different SWB material changes the surface smoothness, for which the friction drag varies in the least amount with the NC result. These minimal variations of the aerodynamic coefficient establish the use of AbCRC as the cost-benefit is more for the SWB material. The other fatigue properties are also justified for AbCRC23.

3.2 Flow field characteristics

The main focus regarding the wind velocity field is the above zone of the box girder. The first investigation is the effect of inlet wind speed (U0) above the deck. Figure 4(a) shows the typical streamwise velocity contour, and Fig. 4(b) and 4(c) shows the critical normalised mean streamwise velocity profile (NVP) for different ICFD models for 47m/s and 61.1m/s wind speed. The NVP is the ratio between U(z)/U0, where U(z) is used for the mean streamwise velocity at height 'z' over the deck surface[36]. The representative velocity contour shows when the maximum drag force acts on the deck, and the streamlined velocity profile shows at the top when velocity acts on 20M_AbCRC at 47ms wind speed. The trapezoidal box girder bridge is a bluff body; therefore, a vortex has also occurred in some cases. The progress on wind environment also increases on 20M_AbCRC compared to other ICFD models for 47m/s. Significantly, NVP shows a good agreement with the different ICFD models. The NVP are 0.88,

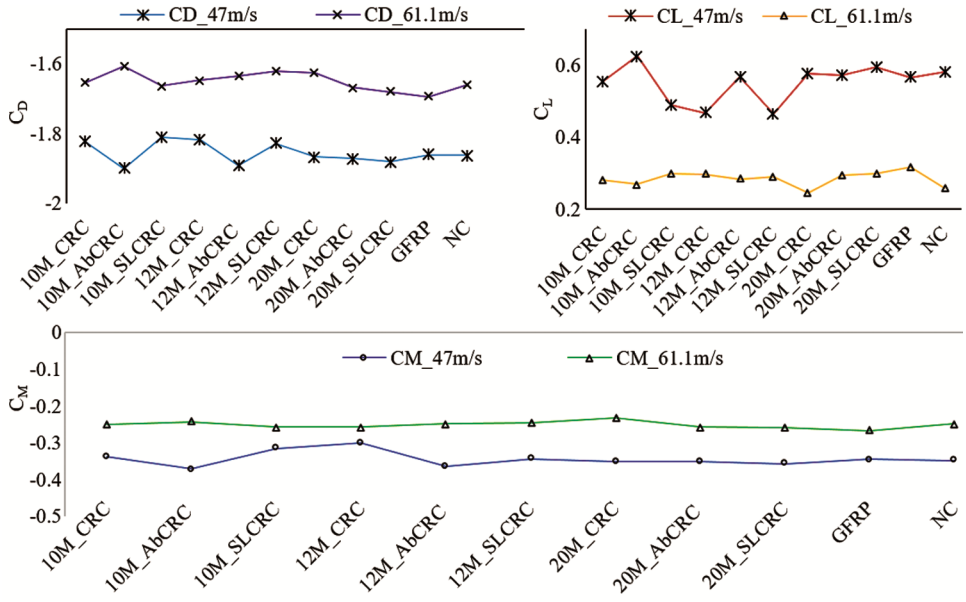

Fig. 3 — Force and moment coefficient for different materials and wind speed.

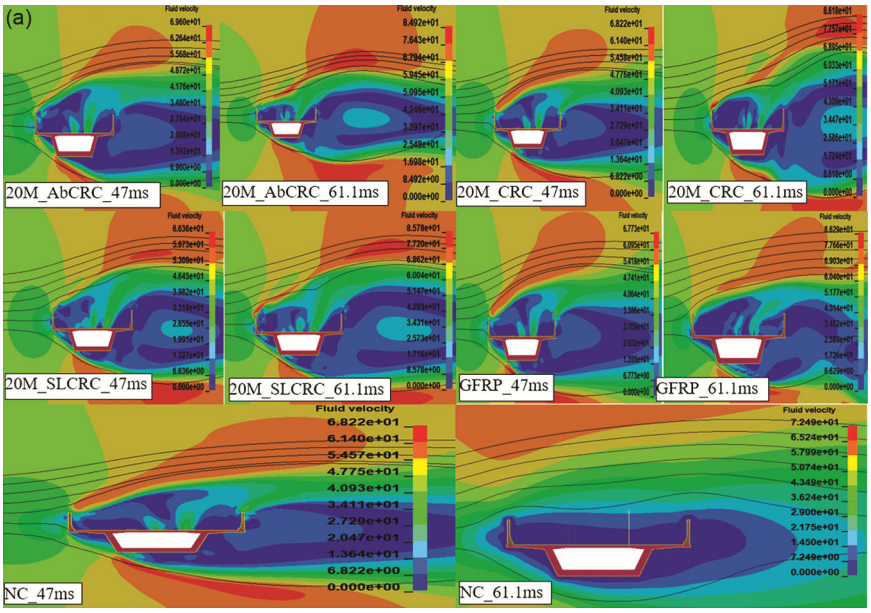

Fig. 4(a) — Contour of the mean streamwise velocity.

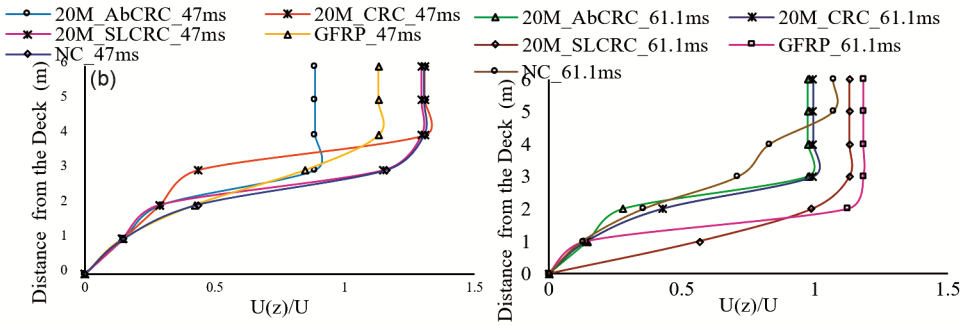

Fig. 4 — (b) NVP for different ICFD models for 47ms, and (c) NVP for different ICFD models for 61.1ms.

0.43, 1.16, 0.84 and 1.16 at z height 3m for 20M_AbCRC, 20M_CRC, 20M_SLCRC, GFRP and NC at 47 m/s. The NVP are 0.99, 0.99, 0.71, 1.18 and 1.13 at z height 3m for 20M_AbCRC, 20M_CRC, 20M_SLCRC, GFRP and NC at 61.1 m/s. In summary, CR-based SWB improves the wind environment, which is conducive to driving safety under crosswinds. Figure 4(a) shows the stationary flow field characteristics change as per the wind speed change in its 2D-RANS-based simulated mean wind velocity contour. The parapet protects the windward side as the mean velocity of the incoming flow somewhat drops. A vortex is seen above the deck surface since the separated flow cannot reattach on the leeward side.

3.3 Pressure contour at different wind speeds

Figure 5(a) shows the representative pressure contour of the ICFD model.Thetorsional moment has demonstrated the input energy during a torsional cycle in Figure 5(b).The pressure distribution of the bridge deck is asymmetric about the horizontal axis. The wind action is more significant at the top than the bottom, as shown in Fig. 5(a).The positive pressure values have been observed on the leading edge. Conversely, the leading edge's upper part turns negative. Further, the upstream portion of the top slab has been identified by a negative value. However, it is clear from the negative pressure values at the whole bottom slab that the flow strikes the same section. Also, the upstream lower portion has a smaller negative value of -906 Pa and-1022 Pa at 47m/s wind speed for 20M_AbCRC and 20M_CRC, respectively. The conjunctions between slabs have larger negative values. In contrast, an almost constant value has been noticed on the remaining part of the section's lower face. This pressure contour indicates that both the underside of the leading edge and the upside have marked flow separations[36].

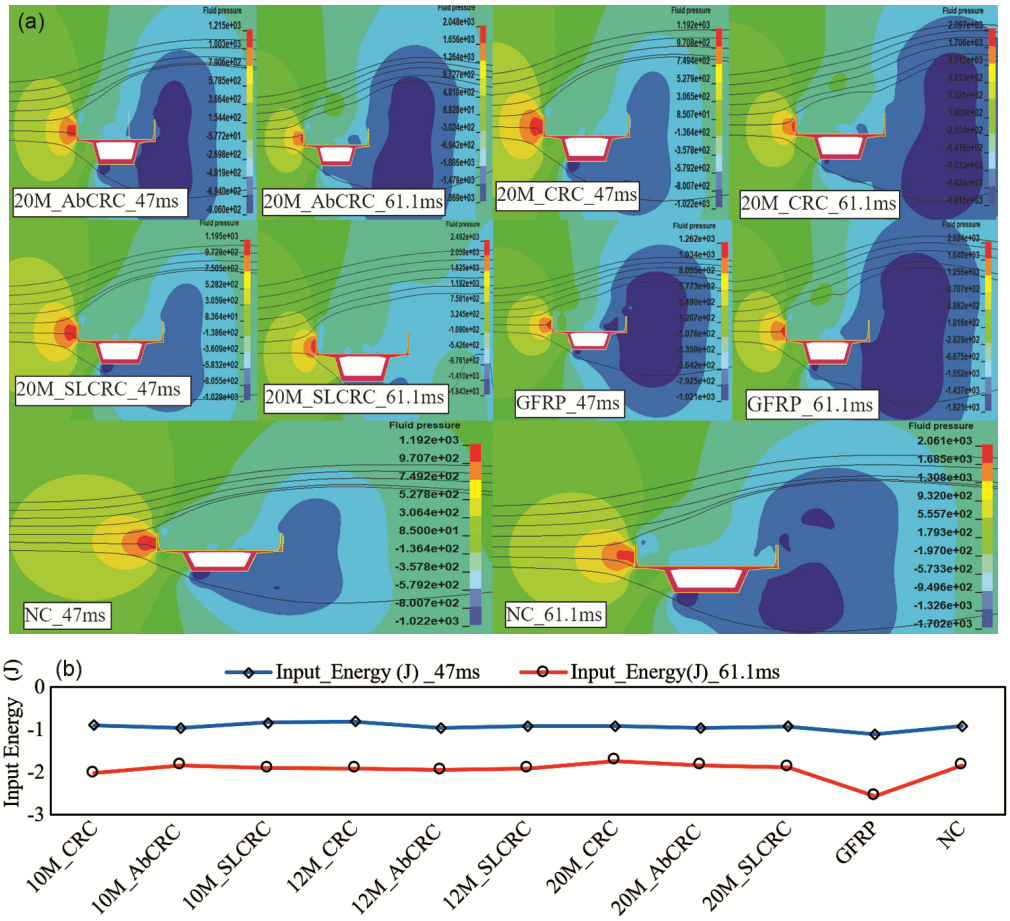

Fig. 5 — ICFD Model (a) Representative pressure contour, and (b) Input energy.

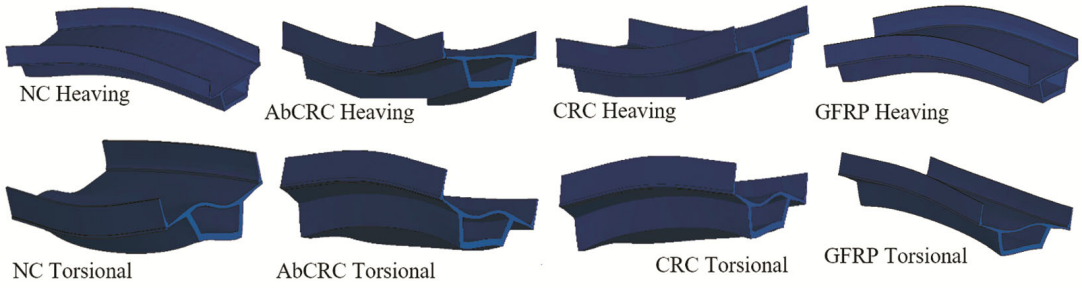

Fig. 6 — The typical mode shape of the different WBM bridge decks.

In order to recognise the aerodynamic mechanism, research has been on the changes in flow field characteristics and the energy input from aerodynamic forces, particularly at different SWB materials. Eq. 5 can be implemented to calculate the SDOF for torsional vibration and the input energy from aerodynamic forces acting on the girder's cross-section periodically.

$$\mathrm{WT} = \int_{t_1}^{t_2} M(t)\, \acute{\alpha}(\mathrm{t})\mathrm{dt5} \qquad \ldots (4)$$

Where t1 and t2 are starting and end times and $\acute{\alpha}(\mathrm{t})$ is the displacement of torsional motion. The vortex behind the model is not regular, as indicated in Fig. 6(a). It clearly means that the input energy is unstable. The GFRP-based SWB model is more varied than the other model. Again, the input energy for the 20M_CRC and 20M_AbCRC models is more significant than the others. The main reason is CR's cushion effect, which bounces back the input energy. The decrement in input energy, especially the

20M_CRC and 20M_AbCRC model, supports using CR in concrete as SWB.

3.4 Modal analysis for various typesof material model

The critical variables for response spectrum and time history research are specifically modal periods.Such methods provide a realistic assessment of the seismic demand and the associated structural response of the bridge. Through the use of modal analysis techniques, the dynamic properties of the bridge structure are explicitly defined. Each vibration mode yields frequencies that depend on the system's mass, stiffness, and damping characteristics. The Heaving and Torsional frequencies are listed in Table 3 and Figure 6 shows the typical mode shape of the different WBM bridge decks. The heaving and torsional frequency is higher for the silica fume and AbCRC thanfor the NC. The relation between the natural frequency and modulus of elasticity (MoE) describes that the increment of MoE increases the natural frequency and vice versa for the material density. Material with high MoE has more resistance to deformation as the stiffness is high and vibratesata higher frequency. Again, low-density material is less massive and vibrates at a higher frequency. SLCRC and AbCRC material-based models have higher MoE than NC and CRC-based models. Therefore, the heaving and rotational frequency increases compared to the NC and CRC-based material models.

3.5 Effect on displacement, velocity and acceleration

Research shows that the stiffness and strength of the wind barrier material are essential to determine its effectiveness. A stiffer and stronger material will withstand higher wind loads and provide better protection to the bridge[37, 38]. Figures 7 a(i-xi), 7b(i-xi) and 7c(i-xi) display the time series of heaving displacement, velocity and acceleration (Acc) of different material models against the two wind speeds. Unlike the SLCRC-based model, the other all-material model has the same type of displacement variation curve in time. Another eye-catching observation is that the displacement variation for increased wind speed is more for NC and 10M_AbCRC than for another material model. Although the MoE is inversely proportional to the displacement, this contradictory increment is shown due to increased wind speed. It also influences the study of spatial displacement concerning this wind speed increment. For the velocity and acceleration case, the increment concerning wind speed has been shown for the 10M_SLCRC and 12M_SLCRC models. However, the bridge is subjected to turbulent wind, which may generate harmonic responses in the structure. Generally, when a wind load acts on a bridge deck, it can vibrate in different modes[39- 42]. If the wind loads have a constant frequency and amplitude, the bridge is excited at one of its natural frequencies or a multiple. Therefore, the bridge response exhibits a sinusoidal pattern, and the amplitude of the response would depend on the wind's magnitude and the bridge's damping characteristics. Figure 7d (i, ii) shows the STD of Rotational and Heaving Displacement and Velocity of 47m/s and 61.1m/s wind speed. Both STDs of heaving and rotational displacement are in a similar trend, i.e. increase with the increase of wind velocity for the 12M_CRC, 12M_AbCRC, 20M_CRC, and 20M_AbCRC material models, a strong coupling between the heaving and rotational displacement. However, the torsional displacement is also dominated by heaving one for the high wind speed, and no non-divergent aerodynamic mechanism has been observed. Further, the result from section 4.2 highlights the studies related to VIV and vortex shredding.

3.6 Overall discussion

The influence of various materials' wind barriers on the aerodynamic and aeroelastic characteristics of TBGB has been explored with ICFD. The flow characteristics have also been investigated. The different material SWB slightly influences the aerodynamic force and moment coefficients. This insignificant impact demonstrates that CD for the material variation on the SWB is not significantly affected by aerodynamic pressure drag force. Pressure

Table 3 — Modal analysis results and shapes for the different WBM bridge deck.

Concrete Name	MoE N/mm2	Frequency in 3D Model		Concrete Name	MoE N/mm2	Frequency in 3D Model	
		Heaving	Torsional			Heaving	Torsional
10M_CRC	27380	3.8948	5.2112	20M_CRC	26920	3.9031	5.2975
10M_AbCRC	30000	3.9349	5.2157	20M_AbCRC	29580	3.9445	5.2155
10M_SLCRC	23700	5.124	5.6774	20M_SLCRC	23900	5.1268	5.6819
12M_CRC	27157	3.9069	5.2932	NC	27950	3.9193	5.2946
12M_AbCRC	29870	3.9329	5.2155	GFRP	8600	3.9445	5.4716
12M_SLCRC	24000	5.1281	5.6841				

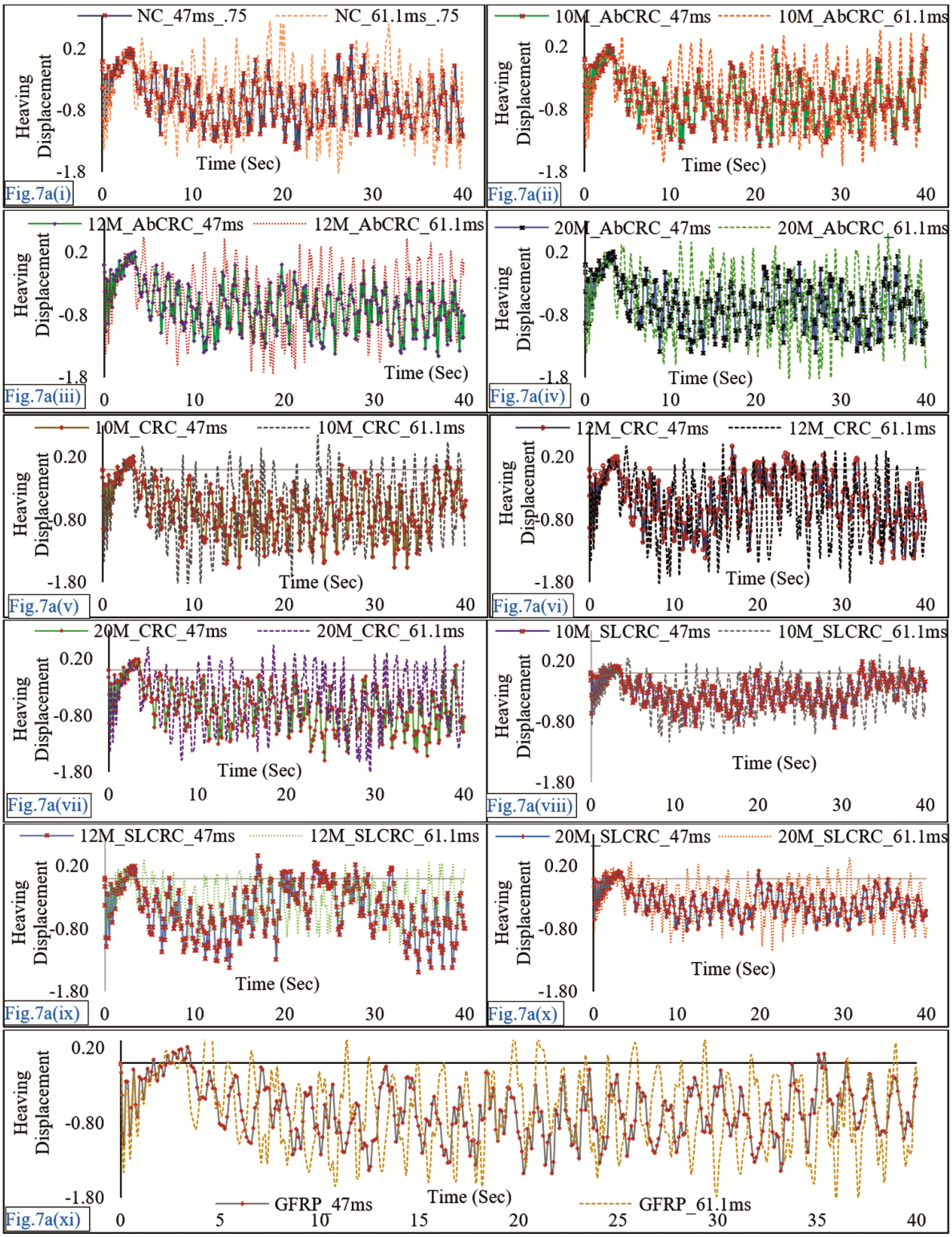

Fig. 7 — (a) Time series of displacement for different material and wind speed (displacement in mm).— (i) Time series of heaving displacement for NC., (ii) 10M_AbCRC., (iii) 12M_AbCRC, (iv) 20M_AbCRC, (v) 10M_CRC, (vi) 12M_CRC, (vii) 20M_CRC, (viii) 10M_SLCRC, (ix) 12M_SLCRC, (x) 20M_SLCRC, and (xi) GFRP.

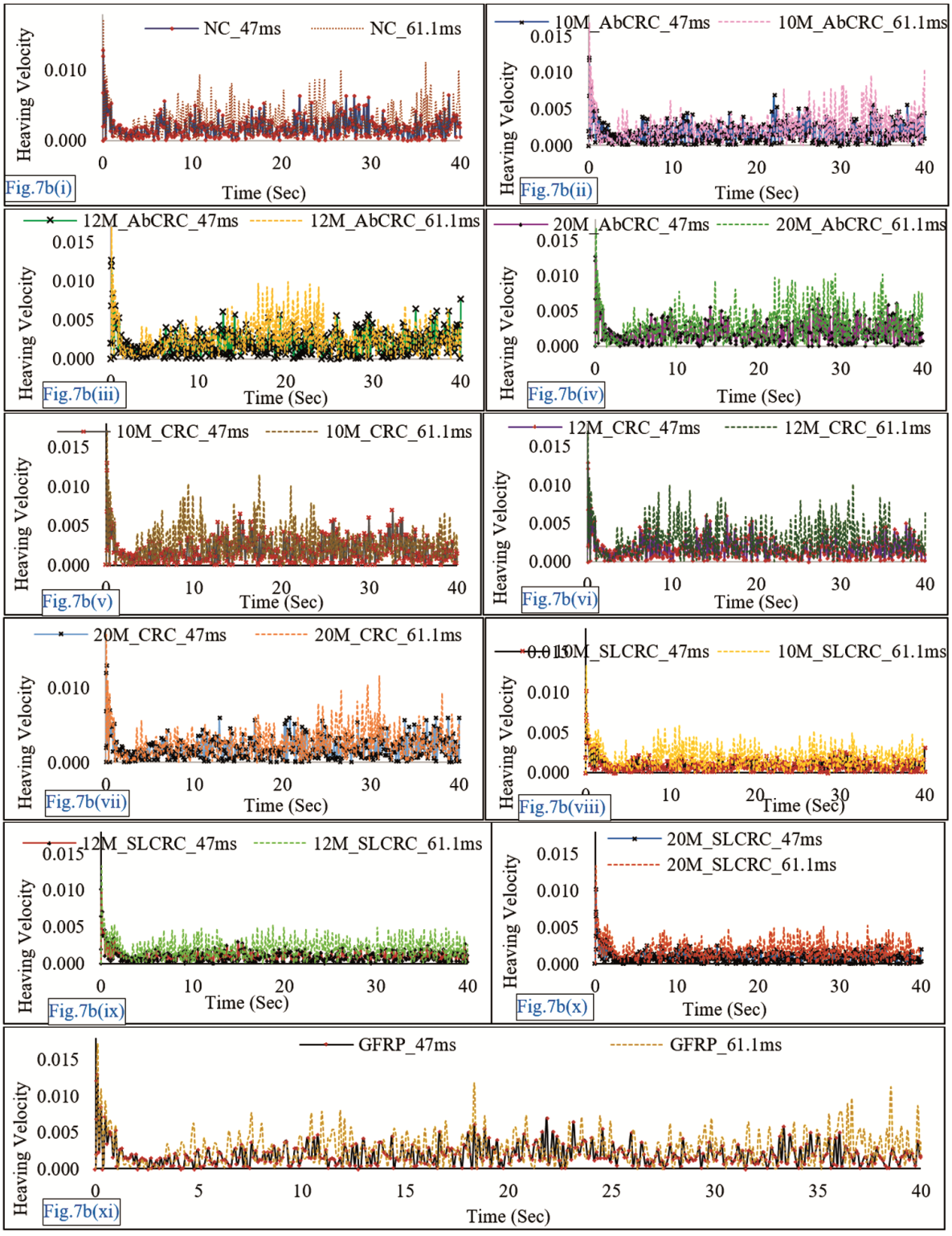

Fig. 7 — (b) Time series of velocity against different material and wind speed (all velocity in m/s). (i) Time series of heaving velocity for NC, (ii) 10M_AbCRC, (iii) 12M_AbCRC, (iv) 20M_AbCRC, (v) 10M_CRC (vi) 12M_CRC, (vii) 20M_CRC, (viii) 10M_SLCRC, (ix) 12M_SLCRC, (x) 20M_SLCRC, and (xi) GFRP.

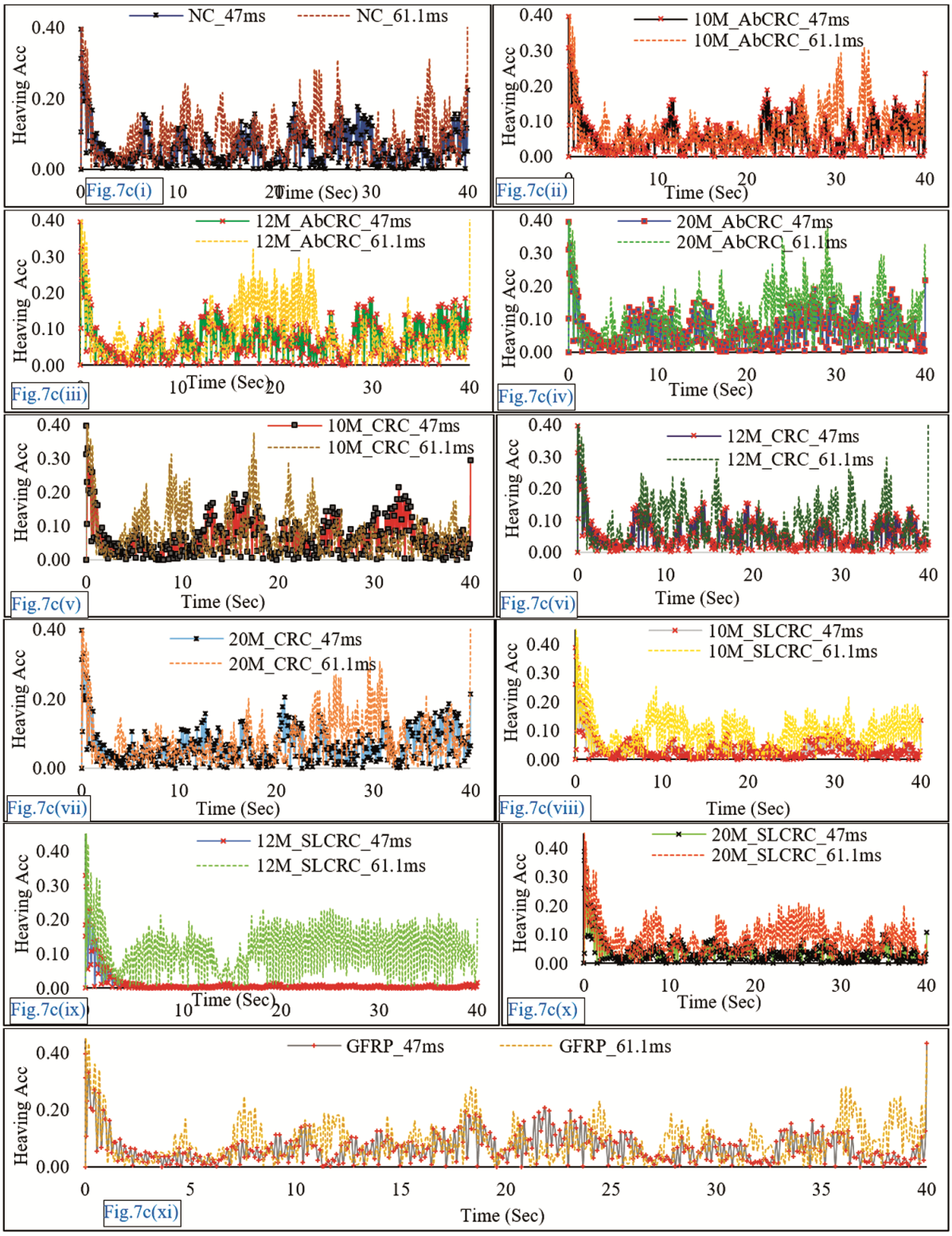

Fig. 7 — (c) Time series of acceleration against different material and wind speeds (acceleration in m/s2). (i) Time series of heaving acceleration for NC. (ii) 10M_AbCRC, (iii) 12M_AbCRC, (iv) 20M_AbCRC, (v) 10M_CRC. (vi) 12M_CRC, (vii) 20M_CRC. (viii) 10M_SLCRC, (ix) 12M_SLCRC (x) 12M_SLCRC, and (xi) GFRP

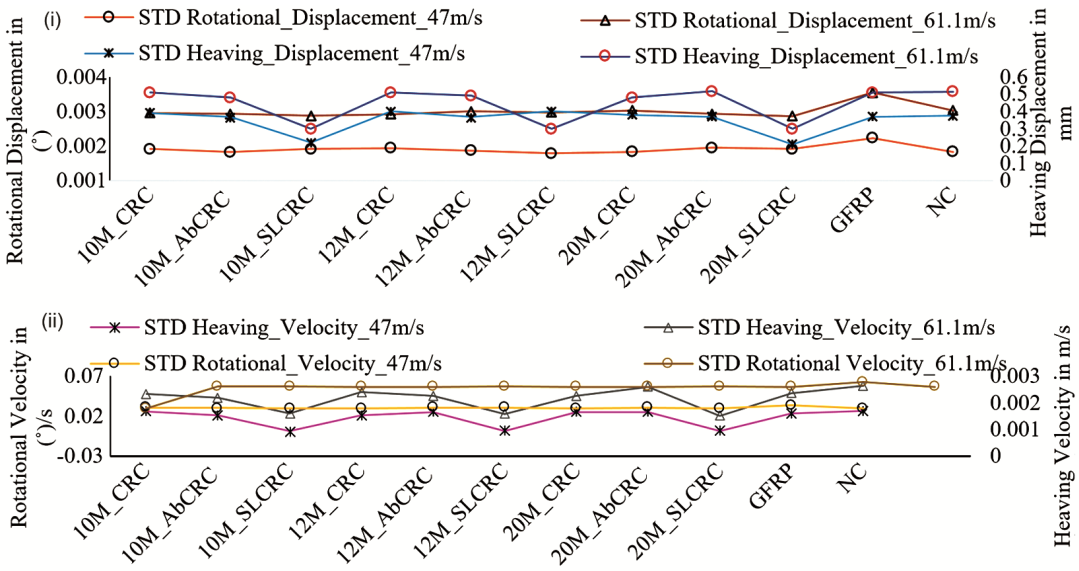

Fig. 7(d) — (i) STD of rotational and heaving displacement of different wind speeds, (ii) STD of rotational and heaving velocity of different wind speeds.

and frictional drag force summation is total drag force. Here, the friction drag varies in the least amount for the change of SWB material compared to NC. Again, compared to other SWB material, AbCRC and its grantable fatigue property are preferable.

The flow separation has been noticed on the leeward side of the bridge cause of the vortex generation. This fatigue effect generator vortex might be for the bluff body section. The parapet provides protection on the windward side when the mean velocity of the incoming flow significantly drops.

20M_CRC and 20M_AbCRC models are more efficient as SWB material as these bounce back the input energy. Regarding displacement variation, the relation to this wind speed increment also encourages the investigation of spatial displacement. In this study, the bridge has been exposed to turbulent wind, which could cause harmonic reactions in the bridge structure. The leeward wind barrier has little impact on bridge deck sections' stability compared to the windward barrier.

4 Conclusion

The proposed SWB material has an adoptive influence on the aerodynamic and aeroelastic characteristics of the SWB of TBGB.Among them, AbCRC has demonstrated its grantability due to its remarkable ability to withstand strain and enhanced ductility, which aid in maintaining progressive collapse. Further, the wind strikes the bottom section of the slab where negative pressure has already been noticed.Repeated occurrence of this effect can be a fatigue problem for the deck, like a vortex, buffeting which is the fatigue generator WIV. Therefore, different measurements for bridge deck materials against the fatigue effect are prescribed. The AbCRC proved itself to be a unique concrete with its excellent fatigue property, which does not affect CD. This characteristic shows a promising possibility of reducing the fatigue on the SWB by applying structural and non-structural parameters.

Moreover, AbCRC lessens the carbon foot print of concrete, making it sustainable. AbCRC thus qualifies as a SWB material, ensuring productive outcomes with minimal adverse effects.

References

1 Dwivedi YK, Shareef MA, Mukerji B, Rana NP & Kapoor KK, *Int J Prod Res,* 56 (2018) 6758.
2 Sharma SK, Misra SK & Singha JB, *Int J Inf Manag,* 51 (2020) 102030.
3 Shanmugasundaram J, Arunachalam S, Gomathinayagam S, Lakshmanan N & Harikrishna P, *J Wind Eng Ind,* 84 (2000) 369.
4 Fakhruddin B, Kintada K & Hassan Q, *Prog Disaster Sci,* (2022) 100216.
5 IMD (2020) Press Release of India Meteorological Department on 20th May 2020.
6 Xianga H, Lia Y, Chen S & Hou G, *Engg Struct,*156 (2018) 188.
7 Buljac A, Kozmar H, Pospísil S & Machacek M, *J Wind EngIndAerod,* 137 (2017) 310.
8 Haldar P & Karmakar S, *J InsEng India Ser A,* 103 (2022) 943.

9 Azunna SU, Aziz FNAA, Rashid RSM & Bakar NBA, *Cleaner Materials*, 12 (2024) 100237.
10 Puram A, Adepu R, Siempu R & Kurre SS, *J Inst Eng (India): A,* 105 (2024) 151.
11 Kinjawadekar TA, Patil S & Nayak G, *J InstEng (India): A,* 104 (2023) 501.
12 Sekhar SS, Patra RK & Mukharjee BB, *Proc Inst Civ Eng.: Eng Sustain*, 177 (2023) 39.
13 Ok B, Sarici T, Demir A, Talaslioglu T & Yildiz A, *Inst Civ Eng: Eng Sustain*, 176 (2022) 285.
14 Tiwari S & Gangwar P, *Mater Today Proc,* 47 (2021) 3778.
15 Yang G, Chen X, Xuan W & Chen Y, *Sadhna,* 43 (2018) 0178.
16 Eldin NN & Senouci AB, *Can J Civ Eng*, 19 (1992) 912.
17 Malarvizhi G, Senthil GN & Kamaraj C, *Int J Sci Res,* 2 (2012) 1.
18 Thomas BS, Gupta RC, Kalla P & Cseteneyi L, *Constr Build Mater*, 59 (2014) 204.
19 Hasan Z, Ahmad G & Amir A, *J Mater Civ Eng,* 28 (2016) 04016156.
20 Roychand R, Gravina RJ, Zhuge Y ,*Constr Build Mater,* 237 (2020) 117651.
21 Shafieyzadeh M, *IJCSM,*7 (2013) 295.
22 Haldar P & Karmakar S, *Proc Inst Civ Eng: Eng Sustain*, 174 (2021) 235.
23 Haldar P & Karmakar S, *Can J Civ Eng, (2024)* (in press).
24 Gupta N, Kishore K, Saxena KK & Joshi TC, *IJEMS*, 28 (2021) 433.
25 Muttil N, Chaudhary S, Prasad KE & Singh SK, *IJEMS*, 29 (2022) 707.
26 Chandak M, Pawade PY & Dhoble RM, *IJEMS*, 30 (2023) 862.
27 Haldar P & Karmakar S, *Sadhana*. 48 (2023) 74.
28 IS: 875 - 2016 (III) Indian Standard Code of Practice for Design Loads (other than Earthquake) for Buildings and Structures, Wind Loads, India.
29 Wu Y, Crawford JE & Magallanes JM, *12th International LS-DYNA Users Conference,* (2012).
30 Madurapperuma M & Niwa K, *AMM*, 566 (2014)173.
31 Tang H, Shum KM & Li Y, *J Wind Eng Ind Aerodyn,* 186 (2019) 192.
32 Tang H, Zhang H & Mo W, *Wind Struct,* 32 (2021) 509.
33 Han Y, Chen H, Cai C, Xu G, Shen L & Hu P, *J Wind EngIndAerod*, 159 (2016) 65.
34 Rocchi D, Argentini T & Sbrosi M, *J Bridge Eng,* 20 (2015) 1.
35 Karmakar S, *Int J Earth sci Eng,* 5(6) (2012) 1708.
36 Guo J, Tang H Li Y & Wang Z, *Adv Struct Eng,* 24 (2020) 453.
37 Buljac A, Kozmar H, Pospíšil S, Macháček M & Kuznetsov S, *J Bridge Eng*, 25 (2020) 04020102.
38 Yang Y, Zhu J, Hong L, Ge Y, Su R, Yang H & Zhou R, *J Bridge Eng*, 28 (2023).
39 Amin J, *J InstEng (India): A,* 104 (2023) 953.
40 Paswan AP, Jayant B, Rukhaiyar A, Dahiya K, Raj R & Menna RK, *J InstEng (India): A,* 104 (2023) 841.
41 Tang H, Li Y & Shum KM, Adv Struct Eng, 21(2018) 335.
42 Roy AK, Yadav H, Dasu SC, Kumar P & Chanotra A, *Asian J CivEng*, 24(2023) 2959.